

# Visualization of all two-qubit states via partial-transpose-moments

Lin Zhang<sup>1\*</sup>, Yi Shen<sup>2†</sup>, Hua Xiang<sup>3</sup>, Quan Qian<sup>1</sup>, Bo Li<sup>1</sup>

<sup>1</sup>*School of Science, Hangzhou Dianzi University, Hangzhou 310018, PR China*

<sup>2</sup>*School of Science, Jiangnan University, Wuxi 214122, PR China*

<sup>3</sup>*School of Mathematics and Statistics, Wuhan University, Wuhan 430072, PR China*

July 12, 2023

## Abstract

Efficiently detecting entanglement based on measurable quantities is a basic problem for quantum information processing. Recently, the measurable quantities called partial-transpose (PT)-moments have been proposed to detect and characterize entanglement. In the recently published paper [L. Zhang *et al.*, *Ann. Phys.(Berlin)* **534**, 2200289 (2022)], we have already identified the 2-dimensional (2D) region, comprised of the second and third PT-moments, corresponding to two-qubit entangled states, and described the whole region for all two-qubit states. In the present paper, we visualize the 3D region corresponding to all two-qubit states by further involving the fourth PT-moment (the last one for two-qubit states). The characterization of this 3D region can finally be achieved by optimizing some polynomials. Furthermore, we identify the dividing surface which separates the two parts of the whole 3D region corresponding to entangled and separable states respectively. Due to the measurability of PT-moments, we obtain a complete and operational criterion for the detection of two-qubit entanglement.

## 1 Introduction

Quantum entanglement has been regarded as an indispensable resource in various information processing tasks. Nevertheless, the detection and characterization of entanglement is not easy, especially for high-dimensional and multipartite systems. A well-known fact is that to determine a bipartite state is separable or entangled is an NP-hard problem [1, 2, 3]. For this notorious difficulty, the low-dimensional systems, especially the two-qubit system, are still the main setting in quantum experiments [4]. Fortunately, the celebrated PPT (positive-partial-transpose) criterion

---

\*godyalin@163.com

†yishen@jiangnan.edu.cn (corresponding author)

is sufficient and necessary for detecting bipartite entanglement in two-qubit and qubit-qutrit systems [5, 6]. In this paper, we focus on two-qubit states, and characterize both the set of entangled states and that of separable states from a graphical point of view which offers an effective tool to understand entanglement [7].

The PPT criterion is actually a mathematical tool commonly used in the theoretical scenario because the partial transposition is not a physical operation. Theoretically, for a given bipartite state  $\rho_{AB}$  of system  $AB$ , detecting its entanglement by PPT criterion is straightforward to check whether the partial transpose of  $\rho_{AB}$ , denoted by  $\rho_{AB}^\Gamma$ , is still positive semidefinite. Nevertheless, in the practical scenario, the detection of entanglement is not so direct. On the one hand, the partial transposition of an operator cannot be implemented directly in experiments. On the other hand, in actual experiments, the quantum state is unknown, unless the resource-inefficient quantum state tomography is performed [8]. More generally, the realizations of effective entanglement criteria usually consume exponential resources, and efficient criteria often perform poorly without prior knowledge [9]. Therefore, it is more valuable to develop efficient methods of detecting entanglement based on measurable quantities from the perspective of resource conservation.

The so-called *partial transpose moments* (PT-moments) introduced in [8] has recently been recognized as the good measurable quantities to efficiently detect entanglement. The  $k$ -th PT-moment, denoted by  $p_k$ , of a state  $\rho_{AB}$  is defined as the sum of  $k$ th-power of each eigenvalue of  $\rho_{AB}^\Gamma$  for any positive integer  $k$  not greater than the global dimension of the bipartite system  $AB$ . Although the PT-moments are nonlinear functions of the state  $\rho_{AB}$  depending on the spectrum of  $\rho_{AB}^\Gamma$ , it has been shown that the PT-moments can be efficiently measured from randomized measurements which are readily available in NISQ devices [10, 11]. The protocol of determining PT-moments proposed in Ref. [10] is efficient for the following three facts. First, compared with previous proposals, this protocol only requires single-qubit control, and allows for the estimation of many distinct PT-moments from the same data [10]. Second, compared with performing full state tomography to compute PT-moments with high accuracy, this protocol requires less measurements, and the number of required measurements decreases significantly for highly mixed states [10]. Third, the PT-moments are predicted by classical postprocessing of the outcomes from very few random measurements specifically designed in Ref. [11]. It leads to the data processing in this protocol is cheap - both in memory and runtime - and can be massively parallelized [10]. In addition, it is known from [12, 13] that the spectrum of  $\rho_{AB}^\Gamma$  can be completely determined with all known PT-moments. Then the PT-moments provide an operational method of detecting entanglement with the help of PPT criterion. The measurability of PT-moments bridges the practical limitations of the PPT criterion, and allows it to be used for experimental entanglement detection. For this advantage, the PT-moment-based entanglement detection has aroused great interest and been widely investigated recently [14, 15, 16].

Moreover, the PT-moments also provide a characterization of states. It is natural to ask whether there is a separable or entangled state compatible with the given data of PT-moments. Due to the difficulty of measuring all the PT-moments, the authors in [8] characterized the separable states supported on  $\mathbb{C}^d$  using the first three PT-moments, where the first PT-moment is normalized as one. Specifically, it is known from [8] that there is a separable state compatible with the given pair of PT-moments  $(p_2, p_3)$  if and only if  $p_3$  is lower and upper bounded by two functions of variable  $p_2 \in [\frac{1}{d}, 1]$ . In [17] we considered the similar question corresponding to two-qubit entangled states, i.e. whether there is an entangled two-qubit state compatible with the given pair  $(p_2, p_3)$ . We answered the above question by determining the accurate lower bound function for  $p_3$  of variable  $p_2 \in [\frac{1}{3}, 1]$  [17]. Thus, combining with the results corresponding to two-qubit separable states, we have already known the 2D feasible region of  $(p_2, p_3)$  corresponding to all two-qubit states and the dividing curve between the two regions corresponding to separable and entangled states respectively.

The 2D region of  $(p_2, p_3)$  for all two-qubit states is lack of the information of  $p_4$ , and thus it is incomplete and just a projection of the whole 3D region of  $(p_2, p_3, p_4)$ . In order to describe the complete graph of all two-qubit states, we further study the relation between  $p_4$  and the pair  $(p_2, p_3)$  in this paper. The complete graph of all two-qubit states is a 3D region in the  $(p_2, p_3, p_4)$ -coordinate system, where the pair  $(p_2, p_3)$  is restricted in the 2D feasible region above-mentioned [17]. Then the characterization of the complete graph of all two-qubit states can be mathematically formulated as the problem of bounding  $p_4$  with binary functions in terms of two variables  $p_2$  and  $p_3$ , where the pair  $(p_2, p_3)$  is restricted in the feasible region. By virtue of the linear relation between  $p_4$  and the determinant of  $\rho_{AB}^\Gamma$  for the fixed pair  $(p_2, p_3)$ , we equivalently transform the original problem to an optimization problem with respect to a variable  $s$  which is a sum of the largest three eigenvalues of  $\rho_{AB}^\Gamma$ . By figuring out this optimization problem we finally determine the lower bound function  $F^-(p_2, p_3)$  and upper bound function  $F^+(p_2, p_3)$  in Theorem 3.2, such that  $F^-(p_2, p_3) \leq p_4 \leq F^+(p_2, p_3)$  for any fixed pair  $(p_2, p_3)$  in the feasible region. Furthermore, in Proposition 3.4 we identify the border surface which separates the two regions corresponding to entangled and separable states respectively. Due to the measurability of PT-moments, we obtain an operational criterion for the detection of two-qubit entanglement. In order to make the process of deriving  $F^+(p_2, p_3)$  and  $F^-(p_2, p_3)$  clearer, we summarize the calculating procedure of the maximum and minimum values of  $p_4$  for a given pair  $(p_2, p_3)$  in the feasible region. As examples we plot the graph of the family of Werner states and the family of Bell-diagonal states in Figure 1 and Figure 2 respectively, by following the above calculating procedure. Generally, we further visualize the 3D region corresponding to the set of all two-qubit states in Figure 4, and mark the separable region and entangled region in different colors. Finally, we compare the criterion in terms of the triple  $(p_2, p_3, p_4)$  with two common entanglement measures, i.e. the

negativity and the concurrence, and consequently conclude that the criterion proposed in this paper has the same performance as such two entanglement measures in the aspect of detecting two-qubit entanglement.

The paper is organized as follows. In Sect. 2, we mathematically formulate the expression of each PT-moment, recall the feasible region of the pair  $(p_2, p_3)$  specifically, and clarify some essential notations frequently used to derive main results. In Sect. 3, we specifically explain the process of deriving the lower and upper bound functions for  $p_4$  step by step. Some derivation details are put in appendices for simplicity. In Sect. 4, we summarize the calculating procedure of the maximum and minimum values of  $p_4$  when inputting a given pair  $(p_2, p_3)$ . We specifically study two families of states by following the calculating procedure in this section. In Sect. 5, we present the visualization of all two-qubit states via PT-moments. In Sect. 6, we compare our proposed criterion via PT-moments with two common entanglement measures on the entanglement detection. Finally, we conclude in Sect. 7.

## 2 Preliminary

For any bipartite state  $\rho_{AB}$  supported on the Hilbert space  $\mathcal{H}_{AB} \cong \mathbb{C}^{d_A} \otimes \mathbb{C}^{d_B}$ , its PT-moments [8] are defined in terms of the spectrum of its partial transpose  $\rho_{AB}^\Gamma$  with respect to one of both subsystems as:

$$p_k = \text{Tr} \left( \left[ \rho_{AB}^\Gamma \right]^k \right) = \sum_{j=1}^{d_A d_B} x_j^k \quad (1 \leq k \leq d_A d_B) \quad (2.1)$$

where  $x_j$ 's are the eigenvalues of  $\rho_{AB}^\Gamma$  sorted in the descending order. We call  $\mathbf{p}^{(d)} = (p_1, \dots, p_d)$  the PT-moment vector where  $d = d_A d_B$ , and always assume  $p_1 = 1$  for convenience. It follows from [12] that the spectrum of  $\rho_{AB}^\Gamma$  can be completely determined with all known PT-moments, for which whether  $\rho_{AB}$  is an NPT state can be verified.

In this paper, we focus on the two-qubit system. According to the above description, there are four PT-moments in total for any two-qubit state, i.e.  $p_1, p_2, p_3, p_4$  defined by Eq. (2.1). For two-qubit states, we have already identified the 2D region comprised of a pair of PT-moments namely  $(p_2, p_3)$  in our recent paper [17]. In order to obtain a more comprehensive picture of all two-qubit states by PT-moments, we further introduce the fourth PT-moment  $p_4$  to characterize the complete graph of all two-qubit states. Specifically, we shall identify the 3D regions corresponding to the set of entangled states and that of separable states respectively in terms of a triple of PT-moments namely  $(p_2, p_3, p_4)$ . First, we recall the relation between  $p_2$  and  $p_3$  derived in [17], where we bounded  $p_3$  with functions of variable  $p_2$  as follows. It is known from [17] that

$$\frac{1}{4} \leq p_2 \leq 1, \quad f^-(p_2) \leq p_3 \leq f^+(p_2), \quad (2.2)$$

where

$$f^\pm(p_2) = \frac{3(6p_2 - 1) \pm \sqrt{3}(4p_2 - 1)^{\frac{3}{2}}}{24}. \quad (2.3)$$

Denote by

$$\mathcal{A} := \left\{ (p_2, p_3) : \frac{1}{4} \leq p_2 \leq 1, \quad f^-(p_2) \leq p_3 \leq f^+(p_2) \right\} \quad (2.4)$$

the feasible region of the pair of PT-moments  $(p_2, p_3)$  for all two-qubit states. Furthermore, from [17, Fig. 1] there is a curve represented by  $p_3 = \phi_4(p_2)$  which divides the separable part (corresponding to separable states) and entangled part (corresponding to entangled states) of 2D region  $\mathcal{A}$ . The function  $p_3 = \phi_4(p_2)$  has been specifically formulated [17, Eq. (10)] as

$$\phi_4(p_2) = \begin{cases} \frac{3p_2-1}{2}, & p_2 \in [\frac{1}{2}, 1] \\ \frac{2(9p_2-2)-\sqrt{2}(3p_2-1)^{\frac{3}{2}}}{18}, & p_2 \in [\frac{1}{3}, \frac{1}{2}] \\ \frac{3(6p_2-1)-\sqrt{3}(4p_2-1)^{\frac{3}{2}}}{24}, & p_2 \in [\frac{1}{4}, \frac{1}{3}] \end{cases}. \quad (2.5)$$

One can verify that  $\phi_4(p_2) \geq p_2^2$ ,  $\forall p_2 \in [\frac{1}{4}, 1]$ , and the equality holds only when  $p_2 = \frac{1}{4}, \frac{1}{3}, 1$ . Hence, there are infinite pairs  $(p_2, p_3) \in \mathcal{A}$  satisfying  $\phi_4(p_2) > p_3 > p_2^2$  for  $p_2 \in (\frac{1}{3}, 1)$ . Recall that if  $\rho_{AB}$  is PPT, then its pair of PT-moments must satisfy  $p_3 \geq p_2^2$  [10]. Comparing this criterion with the criterion we previously proposed in Ref. [17], there are entangled states which can be detected by  $\phi_4(p_2) > p_3$  but cannot be detected by  $p_3 > p_2^2$ . It shows our previous criterion is more powerful than that in Ref. [10]. Analogous to the 2D region given by  $\mathcal{A}$ , we continue to derive the 3D region comprised of the triple of PT-moments namely  $(p_2, p_3, p_4)$  for all two-qubit states. Because the last PT-moment  $p_4$  for two-qubit states is involved, the 3D region and the entanglement detection criterion in terms of  $(p_2, p_3, p_4)$  should be more complete. For convenience, we introduce some essential notations which will be frequently used in the expression of our main results.

The focused problem is to bound  $p_4$  with binary functions in  $p_2$  and  $p_3$ . According to Eq. (2.1), each PT-moment of a state is closely related to the spectrum of its partial transpose. Denote by  $\rho_{AB}$  an arbitrary two-qubit state, and  $\rho_{AB}^\Gamma$  is the partial transpose. There are some constraints on the spectrum of  $\rho_{AB}^\Gamma$ . It follows from Ref. [18] that  $\rho_{AB}$  is NPT if and only if  $\rho_{AB}^\Gamma$  has exact one negative value, and the eigenvalues of  $\rho_{AB}^\Gamma$  all belong to the interval  $[-\frac{1}{2}, 1]$ . Suppose  $x \geq y \geq z$  are the three nonnegative eigenvalues of  $\rho_{AB}^\Gamma$ , and thus the fourth eigenvalue is  $1 - x - y - z$ . Then for any fixed pair of PT-moments  $(p_2, p_3) \in \mathcal{A}$ , all of three parameters must satisfy the

following constraints:

$$1 \geq x \geq y \geq z \geq 0, \quad (2.6)$$

$$z \geq 1 - x - y - z \geq -\frac{1}{2}, \quad (2.7)$$

$$x^2 + y^2 + z^2 + (1 - x - y - z)^2 = p_2, \quad (2.8)$$

$$x^3 + y^3 + z^3 + (1 - x - y - z)^3 = p_3. \quad (2.9)$$

Define the objective function as  $s \equiv s(x, y, z) := x + y + z$ . For any fixed pair of PT-moments  $(p_2, p_3) \in \mathcal{A}$ , denote by  $\mathcal{V}(p_2, p_3)$  the set of feasible triples  $(x, y, z)$  meeting all the above constraints. As we shall see in Sect. 3, the following two values are essential to derive our main results. For any pair  $(p_2, p_3) \in \mathcal{A}$ , define

$$s_{\max} \equiv s_{\max}(p_2, p_3) := \max_{\mathcal{V}(p_2, p_3)} s(x, y, z), \quad (2.10)$$

$$s_{\min} \equiv s_{\min}(p_2, p_3) := \min_{\mathcal{V}(p_2, p_3)} s(x, y, z). \quad (2.11)$$

Without ambiguity, we may use  $s_{\max}$  and  $s_{\min}$  to denote  $s_{\max}(p_2, p_3)$  and  $s_{\min}(p_2, p_3)$ , respectively.

Although for any given pair  $(p_2, p_3)$ , the two values  $s_{\max}$  and  $s_{\min}$  can be numerically calculated, the analytical expressions of the two functions  $s_{\max}(p_2, p_3)$  and  $s_{\min}(p_2, p_3)$  given by Eqs. (2.10) and (2.11) are quite complicated to derive. Here we made two rough conclusions on  $s_{\max}$  and  $s_{\min}$ . First, combining Eqs. (2.6) and (2.7) leads to  $1 \geq x \geq y \geq z \geq 1 - s \geq -\frac{1}{2}$ . It implies that the value  $s = x + y + z$  satisfies  $s \geq 3(1 - s)$  and  $1 - s \geq -\frac{1}{2}$ . It is not hard to figure out  $s \in [\frac{3}{4}, \frac{3}{2}]$ , and thus  $[s_{\min}, s_{\max}] \subseteq [\frac{3}{4}, \frac{3}{2}]$  from Eqs. (2.10) and (2.11). Second, we claim that the maximum and minimum values  $s_{\max}$  and  $s_{\min}$  are reached only if all of three variables  $x, y, z$  are equal. We present the proof of this claim in Appendix A.

### 3 Characterization of the 3D region in terms of PT-moments

As we have obtained the 2D region comprised of the pair of PT-moments  $(p_2, p_3)$  [17], in order to obtain the whole 3D region comprised of the triple of PT-moments  $(p_2, p_3, p_4)$ , we only need to bound the fourth PT-moments  $p_4$  with binary functions of two variables  $p_2$  and  $p_3$ . In this section we derive the lower bound function  $F^-(p_2, p_3)$  and upper bound function  $F^+(p_2, p_3)$  such that  $F^-(p_2, p_3) \leq p_4 \leq F^+(p_2, p_3)$  for all two-qubit states. Such two functions can be derived through the following steps.

First of all, it follows from Ref. [12] that the determinant of  $\rho_{AB}^\Gamma$  has an analytical expression in terms of  $p_2, p_3, p_4$ , i.e.

$$\det(\rho_{AB}^\Gamma) = \frac{3p_2^2 - 6p_2 + 8p_3 - 6p_4 + 1}{4!}. \quad (3.1)$$

From the above equation we calculate  $p_4$  as

$$p_4 = \frac{3p_2^2 - 6p_2 + 8p_3 + 1}{6} - 4\det(\rho_{AB}^\Gamma). \quad (3.2)$$

Let  $F(p_2, p_3) := \frac{3p_2^2 - 6p_2 + 8p_3 + 1}{6}$ . Then  $p_4$  also reads  $p_4 = F(p_2, p_3) - 4\det(\rho_{AB}^\Gamma)$  for simplicity. Since  $(p_2, p_3) \in \mathcal{A}$  are fixed arbitrarily, it follows from Eq. (3.2) that the maximum of  $p_4$  is achieved if and only if the minimum of  $\det(\rho_{AB}^\Gamma)$  is achieved, and analogously the minimum of  $p_4$  is achieved if and only if the maximum of  $\det(\rho_{AB}^\Gamma)$  is achieved. That is, for any fixed pair  $(p_2, p_3) \in \mathcal{A}$ ,

$$F^+(p_2, p_3) := \frac{3p_2^2 - 6p_2 + 8p_3 + 1}{6} - 4m(p_2, p_3) = F(p_2, p_3) - 4m(p_2, p_3), \quad (3.3)$$

$$F^-(p_2, p_3) := \frac{3p_2^2 - 6p_2 + 8p_3 + 1}{6} - 4M(p_2, p_3) = F(p_2, p_3) - 4M(p_2, p_3), \quad (3.4)$$

where  $m(p_2, p_3)$  and  $M(p_2, p_3)$  are respectively the minimum and maximum of  $\det(\rho_{AB}^\Gamma)$  over those two-qubit states whose second and third PT-moments are respectively equal to the given  $p_2$  and  $p_3$ . Thus, in this first step, we equivalently transform the problem of deriving  $F^+(p_2, p_3)$  and  $F^-(p_2, p_3)$  to the problem of bounding the determinant  $\det(\rho_{AB}^\Gamma)$ .

The second step is to accurately bound  $\det(\rho_{AB}^\Gamma)$ , i.e. the lower bound  $m(p_2, p_3)$  and upper bound  $M(p_2, p_3)$  for any given pair  $(p_2, p_3) \in \mathcal{A}$ . Recall that we have assumed  $x, y, z$  and  $1 - x - y - z$  are the four eigenvalues of  $\rho_{AB}^\Gamma$  in the descending order. It implies  $\det(\rho_{AB}^\Gamma) = xyz(1 - x - y - z)$ . Recall that for any fixed pair  $(p_2, p_3) \in \mathcal{A}$ , the triple of variables  $(x, y, z)$  satisfies the constraints given by Eqs. (2.6) — (2.9). We have already known that  $\rho_{AB}$  is an NPT state if and only if  $\det(\rho_{AB}^\Gamma) < 0$  [18, 19]. It implies that  $\det(\rho_{AB}^\Gamma)$  attains its maximal value on some PPT states, i.e. separable states, and attains its minimal value on some NPT states, i.e., entangled states. Hence, we first propose the global maximal and minimal values of  $\det(\rho_{AB}^\Gamma)$  over the set of all two-qubit states, namely  $\mathcal{D}(\mathbb{C}^2 \otimes \mathbb{C}^2)$ . For any fixed pair  $(p_2, p_3) \in \mathcal{A}$ , we conclude that

$$-\frac{1}{16} \leq m(p_2, p_3) \leq \det(\rho_{AB}^\Gamma) \leq M(p_2, p_3) \leq \frac{1}{256}. \quad (3.5)$$

The specific calculation of the global maximal and minimal values of  $\det(\rho_{AB}^\Gamma)$  is put in Appendix B. Combining the above observation with Eqs. (3.3) — (3.4), we also estimate the difference between  $F^+(p_2, p_3)$  and  $F^-(p_2, p_3)$  as

$$0 \leq F^+(p_2, p_3) - F^-(p_2, p_3) = 4[M(p_2, p_3) - m(p_2, p_3)] \leq \frac{17}{64}, \quad \forall (p_2, p_3) \in \mathcal{A}. \quad (3.6)$$

Next, we shall determine  $m(p_2, p_3)$  and  $M(p_2, p_3)$  accurately for any pair  $(p_2, p_3) \in \mathcal{A}$ . We transform this problem to the optimization problem on the objective function  $P(s|p_2, p_3)$  over the closed interval  $[s_{\min}, s_{\max}]$ , where  $s_{\max}$  and  $s_{\min}$  have been clarified by Eqs. (2.10) and (2.11)



respectively. That is,

$$M(p_2, p_3) = \max_{s \in [s_{\min}, s_{\max}]} \Phi(s|p_2, p_3) = - \min_{s \in [s_{\min}, s_{\max}]} P(s|p_2, p_3), \quad (3.7)$$

$$m(p_2, p_3) = \min_{s \in [s_{\min}, s_{\max}]} \Phi(s|p_2, p_3) = - \max_{s \in [s_{\min}, s_{\max}]} P(s|p_2, p_3), \quad (3.8)$$

where

$$\begin{aligned} P(s|p_2, p_3) &:= -\Phi(s|p_2, p_3) \\ &= s^4 - 3s^3 + \frac{7-p_2}{2}s^2 + \frac{3p_2+2p_3-11}{6}s + \frac{1-p_3}{3}, \end{aligned} \quad (3.9)$$

for  $s \in [s_{\min}, s_{\max}]$ . We put the detailed transformation process in Appendix C.

The third step is to specifically optimize  $P(s|p_2, p_3)$  over  $[s_{\min}, s_{\max}]$ . We consider  $P(s|p_2, p_3)$  as a parametric polynomial with respect to variable  $s$ , and employ the typical method to figure out this optimization problem. We put the specific derivation process in Appendix D. Based on the analytical discussion in Appendix D we can draw the conclusion as follows.

**Proposition 3.1.** *Let  $P(s|p_2, p_3) := s^4 - 3s^3 + \frac{7-p_2}{2}s^2 + \frac{3p_2+2p_3-11}{6}s + \frac{1-p_3}{3}$  be a function of variable  $s$ , where the pair of parameters  $(p_2, p_3)$  are fixed in  $\mathcal{A}$ . Let  $r_1 \geq r_2 \geq r_3$  be the three roots formulated in Eq. (D.16), such that the first derivative  $\frac{d}{ds}P(s|p_2, p_3)$  is zero. Then,*

$$\min_{s \in [s_{\min}, s_{\max}]} P(s|p_2, p_3) = \min \{v_1, v_2, v_3, v_4\}, \quad (3.10)$$

$$\max_{s \in [s_{\min}, s_{\max}]} P(s|p_2, p_3) = \max \{v_1, v_2, v_3, v_4\}. \quad (3.11)$$

where

$$v_1 := P(s_{\max}|p_2, p_3), \quad v_2 := P(\min\{r_1, s_{\max}\}|p_2, p_3),$$

$$v_3 := P(\max\{s_{\min}, r_2\}|p_2, p_3), \quad v_4 := P(s_{\min}|p_2, p_3).$$

Proposition 3.1 tells us that the maximal and minimal values of  $P(s|p_2, p_3)$  over  $[s_{\min}, s_{\max}]$  are both included in a same set with only four values, which is an essential simplification.

The final step is to identify the two boundary functions  $F^-(p_2, p_3)$  and  $F^+(p_2, p_3)$  for the fourth PT-moment  $p_4$ . Due to the equivalent relations built in the first and second steps, we may formulate  $F^-(p_2, p_3)$  and  $F^+(p_2, p_3)$  with the local extreme values of  $P(s|p_2, p_3)$  for  $s \in [s_{\min}, s_{\max}]$ . The results can be summarized in the following theorem.

**Theorem 3.2.** *There is a two-qubit state  $\rho_{AB}$  compatible with the given PT-moment vector  $\mathbf{p}^{(4)} = (p_1, p_2, p_3, p_4)$ , where  $p_1 = 1$ , if and only if  $F^-(p_2, p_3) \leq p_4 \leq F^+(p_2, p_3)$ , where  $(p_2, p_3) \in \mathcal{A}$ , that is,  $p_2, p_3, p_4$  satisfy the following conditions:*

$$\frac{1}{4} \leq p_2 \leq 1, \quad (3.12)$$

$$f^-(p_2) \leq p_3 \leq f^+(p_2), \quad (3.13)$$

$$F^-(p_2, p_3) \leq p_4 \leq F^+(p_2, p_3), \quad (3.14)$$



where  $f^\pm(p_2)$  are given by Eq. (2.3), and  $F^\pm(p_2, p_3)$  are determined by

$$F^-(p_2, p_3) = F(p_2, p_3) + 4 \min_{s \in [s_{\min}, s_{\max}]} P(s|p_2, p_3), \quad (3.15)$$

$$F^+(p_2, p_3) = F(p_2, p_3) + 4 \max_{s \in [s_{\min}, s_{\max}]} P(s|p_2, p_3), \quad (3.16)$$

via

$$F(p_2, p_3) := \frac{3p_2^2 - 6p_2 + 8p_3 + 1}{6}, \quad (3.17)$$

and the two extreme values given by Eqs. (3.10) and (3.11), respectively.

*Proof.* It follows from Ref. [17] that the feasible set of  $(p_2, p_3)$  for all two-qubit states is  $\mathcal{A}$  given by Eq. (2.4). It implies that Eqs. (3.12) and (3.13) are necessarily satisfied. Combining Eqs. (3.4) and (3.7) we obtain the expression of  $F^-(p_2, p_3)$ , i.e. Eq. (3.15). Similarly, combining Eqs. (3.3) and (3.8) we obtain the expression of  $F^+(p_2, p_3)$ , i.e. Eq. (3.16). Furthermore, the two extreme values  $\min_{s \in [s_{\min}, s_{\max}]} P(s|p_2, p_3)$  and  $\max_{s \in [s_{\min}, s_{\max}]} P(s|p_2, p_3)$  has been derived in Proposition 3.1. This completes the proof.  $\square$

**Remark 3.3.** Let

$$\begin{aligned} Q(s|p_2, p_3) &:= F(p_2, p_3) + 4P(s|p_2, p_3) \\ &= 4 \left( s^4 - 3s^3 + \frac{7-p_2}{2}s^2 + \frac{3p_2+2p_3-11}{6}s + \frac{p_2^2-2p_2+3}{8} \right). \end{aligned} \quad (3.18)$$

Then we see that

$$F^{+/-}(p_2, p_3) = \max / \min_{s \in [s_{\min}, s_{\max}]} Q(s|p_2, p_3). \quad (3.19)$$

The conditions given by Eqs. (3.12) - (3.14) determine a 3D region in the  $(p_2, p_3, p_4)$ -coordinate system, which is corresponding to the set of all two-qubit states. Thus, we characterize the 3D region of all two-qubit states via complete PT-moments by Theorem 3.2.

Based on the above result, we can give an operational criterion for the detection of entanglement existing in two-qubit states as follows.

**Proposition 3.4.** (i) The entangled two-qubit state  $\rho_{AB}$  is compatible with a PT-moment vector  $\mathbf{p}^{(4)}$  if and only if

$$F(p_2, p_3) < p_4 \leq F^+(p_2, p_3), \quad \forall (p_2, p_3) \in \mathcal{A}. \quad (3.20)$$

(ii) The separable two-qubit state  $\rho_{AB}$  is compatible with a PT-moment vector  $\mathbf{p}^{(4)}$  if and only if

$$F^-(p_2, p_3) \leq p_4 \leq F(p_2, p_3), \quad \forall (p_2, p_3) \in \mathcal{A}. \quad (3.21)$$

*Proof.* According to Theorem 3.2, it is equivalent to proving any two-qubit state  $\rho_{AB}$  is entangled if and only if the following inequality holds:

$$p_4 > F(p_2, p_3), \quad (3.22)$$

where  $F(p_2, p_3) := \frac{3p_2^2 - 6p_2 + 8p_3 + 1}{6}$ . This follows directly from the fact that

$$\det(\rho_{AB}^\Gamma) = \frac{3p_2^2 - 6p_2 + 8p_3 - 6p_4 + 1}{4!}. \quad (3.23)$$

It follows from [18, 19] that  $\rho_{AB}$  is entangled if and only if  $\det(\rho_{AB}^\Gamma) < 0$ . It follows that  $3p_2^2 - 6p_2 + 8p_3 - 6p_4 + 1 < 0$ , and equivalently Eq. (3.22) holds. This completes the proof.  $\square$

According to Proposition 3.4, we identify the dividing surface represented by  $p_4 = F(p_2, p_3)$  which separates the whole 3D region of all two-qubit states into two parts corresponding to separable states and entangled states respectively.

## 4 Calculating procedure with examples

According to the above discussion, we can list the calculating procedure of  $F^{+/-}(p_2, p_3)$  (corresponding to  $p_4^{\max/\min}$ ) for  $(p_2, p_3) \in \mathcal{A}$ .

---

**Algorithm 1:** The max/min value of  $p_4$

---

**Input:**  $(p_2, p_3) \in \mathcal{A}$

**Output:**  $p_4^{\max/\min}$

- 1 choose randomly  $(p_2, p_3) \in \mathcal{A}$ ;
  - 2 calculate  $s_{\max/\min} \equiv s_{\max/\min}(p_2, p_3)$  via Eqs. (2.10)/(2.11);
  - 3 calculate  $M(p_2, p_3)/m(p_2, p_3)$  via Eqs. (3.7)/(3.8);
  - 4 calculate  $F^\pm(p_2, p_3)$  via Eqs. (3.3)/(3.4);
  - 5 Output  $p_4^{\max} = F^+(p_2, p_3)$  and  $p_4^{\min} = F^-(p_2, p_3)$ .
- 

Following the above calculating procedure, we list some analytical examples in Table 1 below.

In the following we shall discuss two families of states with extensive applications in quantum information processing by virtue of the above calculating procedure.

**Example 4.1** (The family of Werner states). In 1989, Werner analytically constructed a family of  $\mathbf{U} \otimes \mathbf{U}$  invariant states to investigate local hidden variable (LHV) models. As a toy model, we consider the two-qubit Werner states formulated as

$$\rho_W(w) = w|\psi^-\rangle\langle\psi^-| + (1-w)\frac{\mathbf{1}_4}{4} \quad (4.1)$$

$(p_2, p_3) \in \mathcal{A}$	$s_{\min}$	$s_{\max}$	$m$	$M$	$F^-$	$F^+$
$(\frac{1}{4}, \frac{1}{16})$	$\frac{3}{4}$	$\frac{3}{4}$	$\frac{1}{256}$	$\frac{1}{256}$	$\frac{1}{64}$	$\frac{1}{64}$
$(\frac{1}{3}, \frac{5}{36})$	$\frac{5}{6}$	$\frac{5}{6}$	$\frac{1}{432}$	$\frac{1}{432}$	$\frac{7}{108}$	$\frac{7}{108}$
$(\frac{1}{3}, \frac{1}{9})$	1	1	0	0	$\frac{1}{27}$	$\frac{1}{27}$
$(\frac{1}{2}, \frac{6+\sqrt{3}}{24})$	$\frac{9+\sqrt{3}}{12}$	$\frac{9+\sqrt{3}}{12}$	$\frac{2\sqrt{3}-3}{576}$	$\frac{2\sqrt{3}-3}{576}$	$\frac{7+2\sqrt{3}}{48}$	$\frac{7+2\sqrt{3}}{48}$
$(\frac{1}{2}, \frac{1}{4})$	1	$\frac{3+\sqrt{2}}{4}$	$-\frac{1}{256}$	0	$\frac{1}{8}$	$\frac{9}{64}$
$(\frac{1}{2}, \frac{6-\sqrt{3}}{24})$	$\frac{3+\sqrt{3}}{4}$	$\frac{3+\sqrt{3}}{4}$	$-\frac{2\sqrt{3}+3}{576}$	$-\frac{2\sqrt{3}+3}{576}$	$\frac{7-2\sqrt{3}}{48}$	$\frac{7-2\sqrt{3}}{48}$
$(1, 1)$	1	1	0	0	1	1
$(1, \frac{1}{4})$	$\frac{3}{2}$	$\frac{3}{2}$	$-\frac{1}{16}$	$-\frac{1}{16}$	$\frac{1}{4}$	$\frac{1}{4}$

Table 1: Specific examples with analytical computations

where  $|\psi^-\rangle = \frac{|01\rangle - |10\rangle}{\sqrt{2}}$  and  $w \in [0, 1]$ . By calculation, the 2nd, 3rd, and 4th PT-moments of two-qubit Werner state  $\rho_W(w)$  are, respectively,

$$\begin{cases} p_2 = \frac{1+3w^2}{4} \\ p_3 = \frac{-6w^3+9w^2+1}{16} \\ p_4 = \frac{21w^4-24w^3+18w^2+1}{64} \end{cases} \quad (w \in [0, 1])$$

The region for the family of Werner states in the  $(p_2, p_3, p_4)$ -coordinate system is just a curve, which is visualized in the following Figure 1.

**Example 4.2** (The family of Bell-diagonal states). The Bell-diagonal states [6] in the two-qubit system can be written as

$$\rho_{\text{Bell}} = \frac{1}{4}(\mathbf{1}_4 + \sum_{i=1}^3 t_i \sigma_i \otimes \sigma_i), \quad (4.2)$$

where  $\sigma_i$  for  $i = 1, 2, 3$  are the three Pauli operators as  $\sigma_1 = |0\rangle\langle 1| + |1\rangle\langle 0|$ ,  $\sigma_2 = i|0\rangle\langle 1| - i|1\rangle\langle 0|$ ,  $\sigma_3 = |0\rangle\langle 0| - |1\rangle\langle 1|$ . Hence, a Bell-diagonal state is specified by three real variables  $t_1, t_2$ , and  $t_3$  such that the formula in Eq. (4.2) represents a normalized positive semidefinite operator, which is equivalent to the following constraints:

$$\begin{cases} 1 - t_1 - t_2 - t_3 \geq 0, \\ 1 - t_1 + t_2 + t_3 \geq 0, \\ 1 + t_1 - t_2 + t_3 \geq 0, \\ 1 + t_1 + t_2 - t_3 \geq 0. \end{cases} \quad (4.3)$$

Denote by  $D_{\text{Bell}}$  the set of tuples  $(t_1, t_2, t_3)$  satisfying the above system of inequalities. Because all the four eigenvalues of a two-qubit state are in  $[0, 1]$ , it follows from Eq. (4.2) that  $t_i \in [-1, 1]$

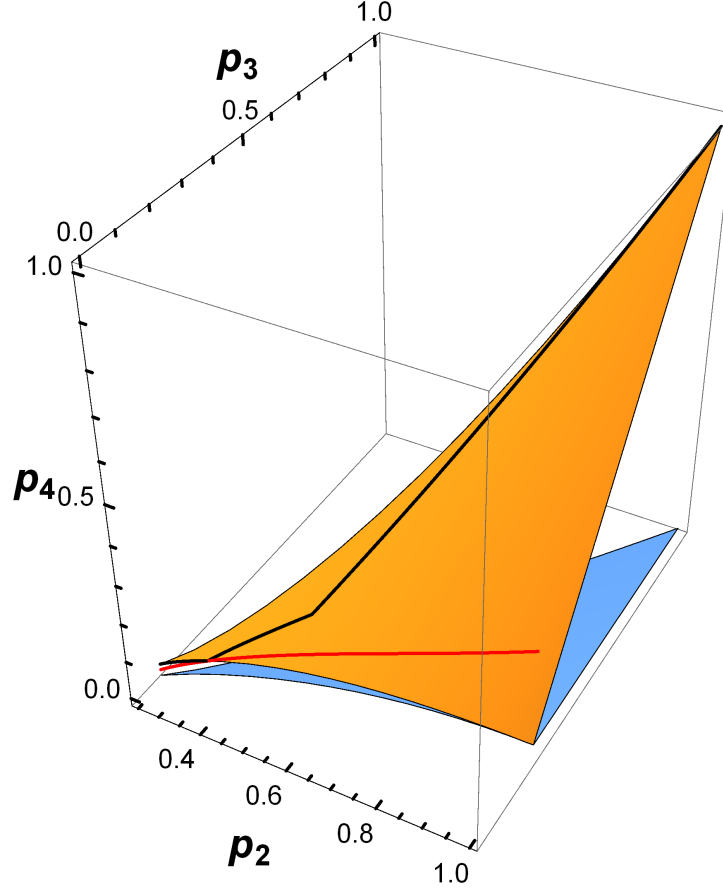


Figure 1: (Color Online) The family of Werner states corresponds to the red curve in the  $(p_2, p_3, p_4)$ -coordinate system, crossing the yellow surface represented by  $p_4 = F(p_2, p_3)$  at the intersection point  $P_0$  with  $(p_2, p_3, p_4) = (\frac{1}{3}, \frac{1}{9}, \frac{1}{27})$ . It is also known from Ref. [17] that in the  $(p_2, p_3)$ -coordinate system the family of Werner states corresponds to the lower boundary curve of 2D region  $\mathcal{A}$  marked in blue on the bottom plane, where  $p_2 \in [\frac{1}{4}, 1]$ . It means that the lower boundary of the blue region is the projection of the red curve. Since the yellow surface  $p_4 = F(p_2, p_3)$  divides the entangled and separable regions, the part of the red curve over the yellow surface (i.e. those points with  $p_2 > \frac{1}{3}$ ) are entangled Werner states, and the part of the red curve below the yellow surface (i.e. those points with  $p_2 \leq \frac{1}{3}$ ) are separable Werner states. Accordingly for the projection of the red curve, the part of the lower boundary curve of the blue region with  $\frac{1}{4} \leq p_2 \leq \frac{1}{3}$  are separable Werner states, and that part with  $\frac{1}{3} < p_2 \leq 1$  are entangled Werner states [17]. In addition, the black curve on the yellow surface is projected as the curve given by  $p_3 = \phi_4(p_2)$  which divides the separable part and entangled part of 2D region  $\mathcal{A}$  [17]. Moreover, the projection of the black curve with  $\frac{1}{4} \leq p_2 \leq \frac{1}{3}$  coincides with the corresponding part of the lower boundary curve of the blue region.

for  $i = 1, 2, 3$ . That is,  $D_{\text{Bell}} \subset [-1, 1]^3$ . Furthermore, the Bell-diagonal states can be graphically described by a tetrahedron. One can show that a Bell-diagonal state is separable if and only if  $|t_1| + |t_2| + |t_3| \leq 1$  holds. Graphically, the set of Bell-diagonal states is a tetrahedron and the set of separable Bell-diagonal states is an octahedron [6], which is denoted by  $D_{\text{Bellsep}}$ . By calculation, all eigenvalues of  $\rho_{\text{Bell}}^\Gamma$  are given by  $\frac{1+t_1-t_2-t_3}{4}, \frac{1-t_1+t_2-t_3}{4}, \frac{1+t_1+t_2+t_3}{4}, \frac{1-t_1-t_2+t_3}{4}$ . It follows from the definition that

$$\begin{cases} p_2 = \frac{1+\sum_{i=1}^3 t_i^2}{4} \\ p_3 = \frac{1+6t_1t_2t_3+3\sum_{i=1}^3 t_i^2}{16} \\ p_4 = \frac{1+24t_1t_2t_3+6\sum_{i=1}^3 t_i^2+\sum_{i=1}^3 t_i^4+6\sum_{1 \leq i < j \leq 3} t_i^2 t_j^2}{64} \end{cases} \quad (4.4)$$

By virtue of the parametric equations formulated in Eq. (4.4), we can draw the 3D region corresponding to the family of Bell-diagonal states in the  $(p_2, p_3, p_4)$ -coordinate system, as depicted in Figure 2 below. We also distinguish the separable region vs entangled region for the family of

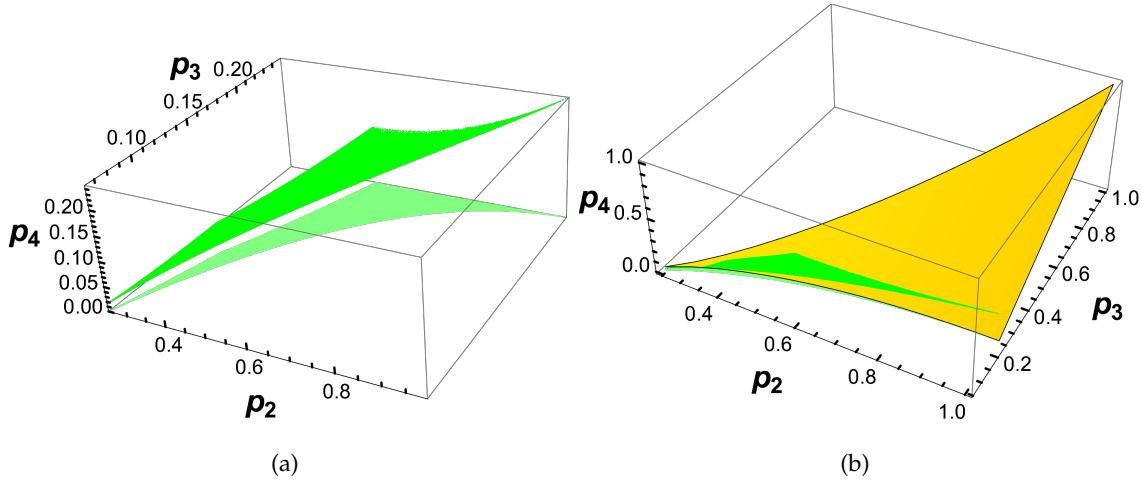


Figure 2: (Color Online) (a) The upper region in green comprised of  $(p_2, p_3, p_4)$  corresponds to the family of Bell-diagonal states, and the lower region in light green is 2D comprised of  $(p_2, p_3)$  and is the projection of the upper region; (b) The dividing yellow surface represented by  $p_4 = F(p_2, p_3)$  crosses the green region of  $(p_2, p_3, p_4)$ . Those points over the surface  $p_4 = F(p_2, p_3)$  correspond to entangled Bell-diagonal states; those ones under the surface  $p_4 = F(p_2, p_3)$  correspond to separable Bell-diagonal states.

Bell-diagonal states, see Figure 3.

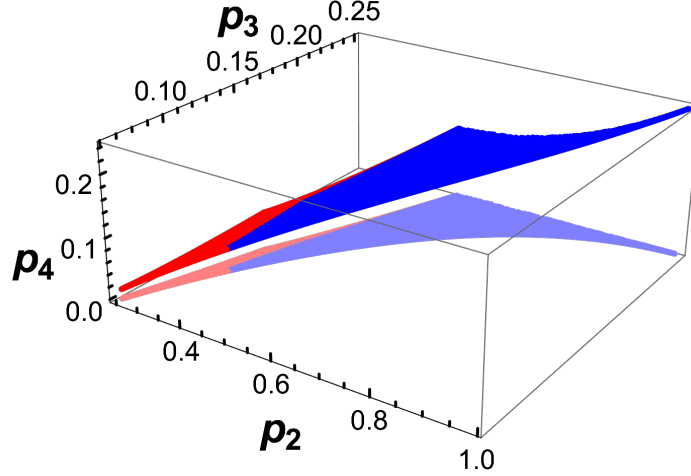


Figure 3: (Color Online) For the family of Bell-diagonal states, the red (blue) 3D region comprised of  $(p_2, p_3, p_4)$  corresponds to separable (entangled) states with their projected regions comprised of  $(p_2, p_3)$  marked in light red (blue).

## 5 Visualization of the 3D region of all two-qubit states

As shown in Figure 1, Figure 2 and Figure 3, we have visualized the 3D regions corresponding to the family of Werner states and that of Bell-diagonal states. In this section we further visualize the 3D region in the  $(p_2, p_3, p_4)$ -coordinate system corresponding to the set of all two-qubit states in Figure 4, according to Theorem 3.2. Based on Proposition 3.4, we identify the separable region (corresponding to the set of separable states) and the entangled region (corresponding to the set of entangled states), and mark such two regions in red and blue respectively in Figure 4 (a). We also add the yellow surface represented by  $p_4 = F(p_2, p_3)$  in Figure 4 (b), which crosses the 3D region and divides the separable and entangled regions.

Finally, we note that the 3D region comprised of  $(p_2, p_3, p_4)$  in Figure 4 is bounded by the two surfaces  $S_+$  and  $S_-$  defined below:

$$S_+ : \quad p_4 = F(p_2, p_3) + \frac{1}{4}, \quad (5.1)$$

$$S_- : \quad p_4 = F(p_2, p_3) - \frac{1}{64}. \quad (5.2)$$

It follows from Eq. (3.5) that  $m(p_2, p_3)$  is lower bounded by  $-\frac{1}{16}$  and  $M(p_2, p_3)$  is upper bounded by  $\frac{1}{256}$ . Substituting such two bounds into Eqs. (3.3) and (3.4) respectively, we conclude that

$$F(p_2, p_3) - \frac{1}{64} \leq F^-(p_2, p_3) \leq F^+(p_2, p_3) \leq F(p_2, p_3) + \frac{1}{4}. \quad (5.3)$$

Graphically, the 3D region comprised of  $(p_2, p_3, p_4)$  corresponding to the set of all two-qubit states is lower bounded by  $S_-$  and upper bounded by  $S_+$ .

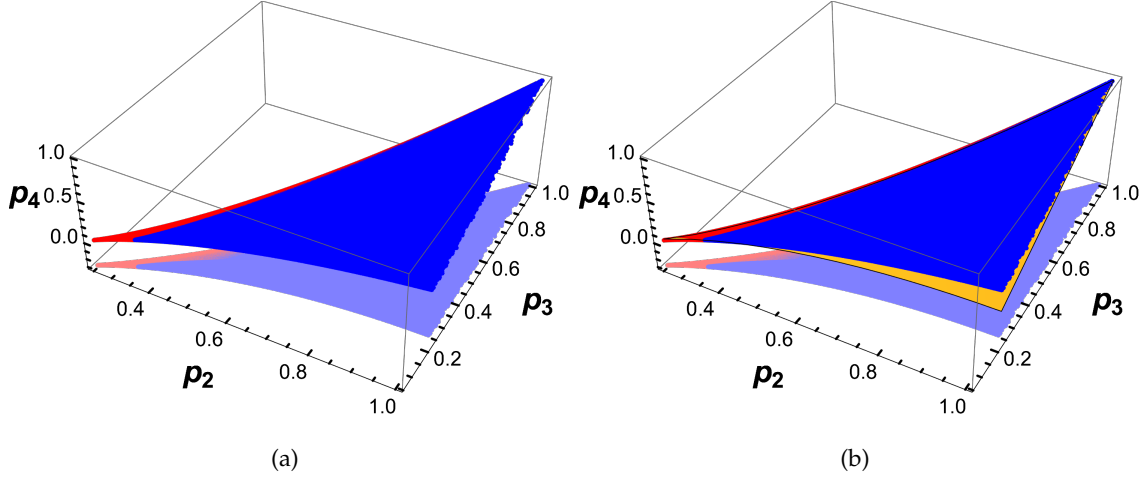


Figure 4: (Color Online) (a) The red (blue) 3D region of  $(p_2, p_3, p_4)$  corresponds to the set of all two-qubit separable (entangled) states with their projections of  $(p_2, p_3)$  marked in light red (blue) on the plane  $p_4 = -0.3$ ; (b) The dividing surface  $p_4 = F(p_2, p_3)$  in yellow crosses the 3D region of  $(p_2, p_3, p_4)$ .

## 6 Comparison between PT-moments and some entanglement measures on the entanglement detection

Negativity and concurrence are two common entanglement measures which have been widely investigated. For any entanglement measure  $E$ ,  $E(\rho_{AB})$  is equal to zero if the state  $\rho_{AB}$  is separable, and  $E(\rho_{AB})$  is greater than zero if the state  $\rho_{AB}$  is entangled. Thus, an analytically computable entanglement measure is also an effective tool to detect entanglement. In this section we shall compare PT-moments and concurrence in the aspect of detecting two-qubit entanglement, via the computable entanglement measure, i.e. the negativity.

For two-qubit states, it is known from Ref. [20] that the negativity (denoted by  $\mathcal{N}$ ) and the concurrence (denoted by  $C$ ) have the following relation:

$$\sqrt{(1 - C)^2 + C^2} - (1 - C) \leq \mathcal{N} \leq C. \quad (6.1)$$

According to this relation, one can verify that  $\mathcal{N}(\rho_{AB}) = 0$  if and only if  $C(\rho_{AB}) = 0$ , and  $\mathcal{N}(\rho_{AB}) > 0$  if and only if  $C(\rho_{AB}) > 0$ . Moreover, due to the PPT criterion on two-qubit states, we conclude that  $\mathcal{N}(\rho_{AB}) = 0$  if and only if  $\rho_{AB}$  is separable. Therefore, using the concurrence to detect two-qubit entanglement is as powerful as using the negativity, although the values of the two measures on some entangled state could be different. Based on this fact, we may use the negativity as an intermediate parameter to discuss the relation between concurrence and PT-moments. Both the negativity and the PT-moment are defined by the eigenvalues of  $\rho^T$ . Here



we assume that  $\lambda_1, \dots, \lambda_4$  are the four eigenvalues of  $\rho^\Gamma$  in the descending order. Denote the elementary symmetric polynomials of  $\lambda_1, \dots, \lambda_4$  by  $e_1, \dots, e_4$ , i.e.

$$e_1 = \sum_{k=1}^4 \lambda_k, \quad e_2 = \sum_{1 \leq i < j \leq 4} \lambda_i \lambda_j, \quad e_3 = \sum_{1 \leq i < j < k \leq 4} \lambda_i \lambda_j \lambda_k, \quad e_4 = \prod_{k=1}^4 \lambda_k. \quad (6.2)$$

If we get measured all PT-moments  $p_1, p_2, p_3, p_4$  with the first PT-moment fixed by constant 1, then we can employ the following formulae [13]

$$e_k = \frac{1}{k!} \begin{vmatrix} p_1 & 1 & 0 & \cdots & 0 \\ p_2 & p_1 & 2 & \cdots & 0 \\ \vdots & \vdots & \vdots & \ddots & \vdots \\ p_{k-1} & p_{k-2} & p_{k-3} & \cdots & k-1 \\ p_k & p_{k-1} & p_{k-2} & \cdots & p_1 \end{vmatrix} \quad (k \geq 1) \quad (6.3)$$

to calculate the value for each  $e_k$ . Then we construct the 4th-order polynomial equation as

$$x^4 - e_1 x^3 + e_2 x^2 - e_3 x + e_4 = 0. \quad (6.4)$$

According to the relationship between roots and coefficients, the four roots of Eq. (6.4) are  $\lambda_1, \dots, \lambda_4$ , and thus we can numerically calculate  $\lambda_1, \dots, \lambda_4$  for measured  $p_1, p_2, p_3, p_4$ . For two-qubit state  $\rho_{AB}$  we have  $\mathcal{N}(\rho_{AB}) = \max(0, -2\lambda_{\min})$ . When  $p_2, p_3, p_4$  satisfy  $F^-(p_2, p_3) \leq p_4 \leq F(p_2, p_3)$  for  $(p_2, p_3) \in \mathcal{A}$ , the state  $\rho_{AB}$  is separable, and thus all eigenvalues  $\lambda_k$  are positive, which leads to  $\mathcal{N}(\rho_{AB}) = 0$ . When  $p_2, p_3, p_4$  satisfy  $F(p_2, p_3) < p_4 \leq F^+(p_2, p_3)$  for  $(p_2, p_3) \in \mathcal{A}$ , the state  $\rho_{AB}$  is entangled, and thus there is only one negative eigenvalue namely  $\lambda_4$ , which leads to  $\mathcal{N}(\rho_{AB}) > 0$ . Based on the equivalence between the negativity and the concurrence in the aspect of detecting two-qubit entanglement, we finally obtain the specific relation between PT-moments and the concurrence as follows.

- $F^-(p_2, p_3) \leq p_4 \leq F(p_2, p_3)$  for  $(p_2, p_3) \in \mathcal{A}$  if and only if  $C = 0$ ;
- $F(p_2, p_3) < p_4 \leq F^+(p_2, p_3)$  for  $(p_2, p_3) \in \mathcal{A}$  if and only if  $C > 0$ .

This tells us that the sign of  $p_4 - F(p_2, p_3)$  can play the role of an entanglement witness as the concurrence. If the sign is  $+1$ , it means the two-qubit state is entangled. Otherwise, it means the two-qubit state is separable. Although the criterion via PT-moments has the same performance as the concurrence and equivalently the negativity in the aspect of detecting two-qubit entanglement, there is a unique advantage of using PT-moments. That is, both the separable and entangled regions can be visualized in the  $(p_2, p_3, p_4)$ -coordinate. This is also a major motivation of this work.

## 7 Conclusion

In this paper, we investigated the characterization of two-qubit states using all PT-moments. Based on the relation between the second and third PT-moments, i.e.,  $p_2$  and  $p_3$  derived in Ref. [17], we further involved the last PT-moment  $p_4$  for two-qubit states, and characterized the relation between  $p_4$  and the pair of PT-moments  $(p_2, p_3)$ . It is a graphical characterization of all two-qubit states by plotting the 3D region comprised of  $(p_2, p_3, p_4)$ . Specifically,  $p_4$  can be bounded by two functions in terms of two variables  $p_2$  and  $p_3$ . We formulated the lower bound function  $F^-(p_2, p_3)$  and the upper bound function  $F^+(p_2, p_3)$  which can be numerically calculated for a given pair  $(p_2, p_3)$ . Furthermore, we also identified the function  $F(p_2, p_3)$  which divides the two regions corresponding to the set of separable states and the set of entangled states respectively. Due to the measurability of PT-moments, we provided an operational criterion for the detection of two-qubit entanglement. To clarify how to obtain  $F^-(p_2, p_3)$  and  $F^+(p_2, p_3)$ , we summarized the calculating procedure, and calculated the two bound functions for the family of Werner states and the family of Bell-diagonal states following the calculating procedure. For such two families of states, we plotted the 3D regions accordingly, and marked the dividing surfaces. Generally, we further visualized the 3D region in the  $(p_2, p_3, p_4)$ -coordinate system corresponding to the set of all two-qubit states, and marked the separable region and entangled region in different colors. Finally, we concluded that the criterion we proposed in terms of the triple  $(p_2, p_3, p_4)$  has the same performance as the two common measures, i.e. the negativity and the concurrence, in the aspect of detecting two-qubit entanglement.

## Acknowledgements

This research is supported by Zhejiang Provincial Natural Science Foundation of China under Grant No. LZ23A010005 and by NSFC under Grant No.11971140. YS is supported by the Fundamental Research Funds for the Central Universities under Grant No. JUSRP123029.

## References

- [1] L. Gurvits, Classical deterministic complexity of Edmonds' problem and quantum entanglement, In Proc. of the 35th ACM symp. on Theory of comp. [pages 10-19, New York, 2003. ACM Press.](#)
- [2] L. Gurvits, Classical complexity and quantum entanglement, J. Comput. Sys. Sci. [69, 448\(2004\).](#)

- [3] S. Gharibian, Strong NP-Hardness of the Quantum Separability Problem, arXiv: [0810.4507v5](#)
- [4] D. Bouwmeester, J-W. Pan, K. Mattle, M. Eibl, H. Weinfurter, and A. Zeilinger, Experimental quantum teleportation, *Nature* **390**, 575-579 (1997).
- [5] A. Peres, Separability criterion for density matrices, *Phys. Rev. Lett.* **77**, 1413(1996).
- [6] M. Horodecki, P. Horodecki, R. Horodecki, Separability of mixed states: necessary and sufficient conditions, *Phys. Lett. A* **223**, 1-8(1996).
- [7] I. Bengtsson and K. Życzkowski, *Geometry of Quantum States: An Introduction to Quantum Entanglement*, Cambridge University Press (2017).
- [8] X-D. Yu, S. Imai, O. Gühne, Optimal entanglement certification from moments of the partial transpose, *Phys. Rev. Lett.* **127**, 060504 (2021).
- [9] P. Liu, Z. Liu, S. Chen, X. Ma, Fundamental Limitation on the Detectability of Entanglement, *Phys. Rev. Lett.* **129**, 230503 (2022).
- [10] A. Elben, R. Kueng, H.-Y.R. Huang, R. van Bijnen, C. Kokail, M. Dalmonte, P. Calabrese, B. Kraus, J. Preskill, P. Zoller, and B. Vermersh, Mixed-state entanglement from local randomized measurements, *Phys. Rev. Lett.* **125**, 200501 (2020).
- [11] H.-Y. Huang, R. Kueng, and J. Preskill, Predicting many properties of a quantum system from very few measurements, *Nature Phys.* **16**, 1050 (2020).
- [12] I.G. Macdonald, *Symmetric Functions and Hall Polynomials*, Oxford University Press, 1995, 2nd Edition, Printed in Great Britain.
- [13] J. Duan, L. Zhang, Q. Qian, and S-M. Fei, A characterization of maximally entangled two-qubit states, *Entropy* **24**(2), 247 (2022).
- [14] Z. Liu, Y. Tang, H. Dai, P. Liu, S. Chen, and X. Ma, Detecting entanglement in quantum many-body systems via permutation moments, *Phys. Rev. Lett.* **129**, 260501 (2022).
- [15] T. Zhang, N. Jing, and S-M. Fei, Quantum separability criteria based on realignment moments, *Quant Inf Process* **21**, 276 (2022).
- [16] K-K. Wang, Z-W. Wei, and S-M. Fei, Operational entanglement detection based on  $\Lambda$ -moments, *Euro. Phys. J. Plus* **137**, 1378 (2022).
- [17] L. Zhang, M-J. Zhao, L. Chen, H. Xiang, Y. Shen, A Characterization of Entangled Two-Qubit States via Partial-Transpose-Moments, *Ann. Phys.(Berlin)* **2200289** (2022).

- [18] S. Rana, Negative eigenvalues of partial transposition of arbitrary bipartite states, Phys. Rev. A [87, 054301 \(2013\)](#).
- [19] Y. Shen, L. Chen, and L-J. Zhao, Inertias of entanglement witnesses, J. Phys. A : Math. Theor. [53, 485302 \(2020\)](#).
- [20] F. Verstraete, K. Audenaert, J. Dehaene and B.D. Moor, A comparison of the entanglement measures negativity and concurrence, J. Phys. A : Math. Gen. [34, 10327-10332\(2001\)](#).
- [21] H.H. Bauschke, M.K. Lal, and X. Wang, Real roots of real cubics and optimization, [arXiv:2302.10731](#)

# Appendices

## A The rough conclusion on $s_{\max}$ and $s_{\min}$

**Lemma A.1.** *The maximum and minimum values  $s_{\max}$  and  $s_{\min}$  defined by Eqs. (2.10) and (2.11) respectively are reached only if at least two of three variables in  $s(x, y, z)$  are equal.*

*Proof.* By using Lagrange Multiplier Method, we define the Lagrange function  $L(x, y, z; \mu, \nu)$  as

$$L(x, y, z; \mu, \nu) = x + y + z + \mu (x^2 + y^2 + z^2 + (1 - x - y - z)^2 - p_2) + \nu (x^3 + y^3 + z^3 + (1 - x - y - z)^3 - p_3). \quad (\text{A.1})$$

In order to get the stationary points, we let all partial derivatives be zero. Then it follows that

$$0 = \frac{\partial L}{\partial x} = 2\mu(2x + y + z - 1) - 3\nu(y + z - 1)(2x + y + z - 1) + 1, \quad (\text{A.2})$$

$$0 = \frac{\partial L}{\partial y} = 2\mu(x + 2y + z - 1) - 3\nu(x + z - 1)(x + 2y + z - 1) + 1, \quad (\text{A.3})$$

$$0 = \frac{\partial L}{\partial z} = 2\mu(x + y + 2z - 1) - 3\nu(x + y - 1)(x + y + 2z - 1) + 1, \quad (\text{A.4})$$

$$0 = \frac{\partial L}{\partial \mu} = x^2 + y^2 + z^2 + (1 - x - y - z)^2 - p_2, \quad (\text{A.5})$$

$$0 = \frac{\partial L}{\partial \nu} = x^3 + y^3 + z^3 + (1 - x - y - z)^3 - p_3. \quad (\text{A.6})$$

The three differences given by (A.2)–(A.3), (A.2)–(A.4), and (A.3)–(A.4) lead to:

$$(x - y)[3\nu(x + y) + 2\mu] = (x - z)[3\nu(x + z) + 2\mu] = (y - z)[3\nu(y + z) + 2\mu] = 0. \quad (\text{A.7})$$

It follows from the above chain of equations that the stationary points satisfy that at least two of three variables  $x, y, z$  are equal.  $\square$

## B The global maximal and minimal values of $\det(\rho_{AB}^\Gamma)$ over all two-qubit states

For the global maximal value, we obtain that

$$\begin{aligned} & \max \left\{ \det(\rho_{AB}^\Gamma) : \rho_{AB} \in D(\mathbb{C}^2 \otimes \mathbb{C}^2) \right\} \\ &= \max \left\{ xyz(1 - x - y - z) : x \geq y \geq z \geq 1 - x - y - z \geq 0 \right\} \\ &= \frac{1}{256}, \end{aligned} \quad (\text{B.1})$$

which is attained only if  $x = y = z = \frac{1}{4}$ . For the global minimal value, we obtain that

$$\begin{aligned}
& \min \left\{ \det(\rho_{AB}^\Gamma) : \rho_{AB} \in \mathcal{D}(\mathbb{C}^2 \otimes \mathbb{C}^2) \right\} \\
&= \min \left\{ xyz(1 - x - y - z) : x \geq y \geq z > 0, 0 > 1 - (x + y + z) \geq -\frac{1}{2} \right\} \\
&= \min \left\{ xyz(1 - x - y - z) : x \geq y \geq z > 0, \frac{3}{2} \geq x + y + z > 1 \right\} \\
&= -\max \left\{ xyz(x + y + z - 1) : x \geq y \geq z > 0, \frac{3}{2} \geq x + y + z > 1 \right\} \\
&= -\frac{1}{16},
\end{aligned} \tag{B.2}$$

which is attained only if  $x = y = z = \frac{1}{2}$ . It implies that  $\det(\rho_{AB}^\Gamma)$  attains its global minimal value if and only if  $\rho_{AB}$  is maximally entangled. Now we conclude that

$$-\frac{1}{16} \leq \det(\rho_{AB}^\Gamma) \leq \frac{1}{256}, \quad \forall \rho_{AB} \in \mathcal{D}(\mathbb{C}^2 \otimes \mathbb{C}^2). \tag{B.3}$$

## C The derivation process of Eqs. (3.7) and (3.8)

Define  $\Phi(x, y, z) := \det(\rho_{AB}^\Gamma) = xyz(1 - x - y - z)$ , where  $x, y, z$  are the largest three eigenvalues of  $\rho_{AB}^\Gamma$ . For any fixed pair  $(p_2, p_3) \in \mathcal{A}$ , the three variables necessarily meet all the constraints given by Eqs. (2.6) — (2.9). Recall the notation  $\mathcal{V}(p_2, p_3)$  introduced below those constraints in Sect. 2. Then we have  $(x, y, z) \in \mathcal{V}(p_2, p_3)$ . Now our optimization problem is formulated as

$$\min / \max \{ \Phi(x, y, z) : (x, y, z) \in \mathcal{V}(p_2, p_3) \}. \tag{C.1}$$

To figure out this optimization problem, let  $s := x + y + z$  be fixed. Using the notations defined by Eqs. (2.10) — (2.11), we obtain that  $s \in [s_{\min}, s_{\max}] \subseteq [\frac{3}{4}, \frac{3}{2}]$ . Then the objective function to be optimized becomes  $\Phi(x, y, z; s) := (1 - s)xyz$ . The problem of optimizing  $\Phi(x, y, z)$  is equivalent to optimizing the objective function  $\Phi(x, y, z; s)$  with respect to  $s \in [s_{\min}, s_{\max}]$  after the optimization of  $\Phi(x, y, z; s)$  with the triple of variables  $(x, y, z)$  subject to the following constraints:

$$x + y + z = s, \tag{C.2}$$

$$1 \geq x \geq y \geq z \geq 0, \tag{C.3}$$

$$z \geq 1 - s \geq -\frac{1}{2}, \tag{C.4}$$

$$x^2 + y^2 + z^2 = p_2 - (1 - s)^2, \tag{C.5}$$

$$x^3 + y^3 + z^3 = p_3 - (1 - s)^3. \tag{C.6}$$

One can verify the following observation:

$$xyz = \frac{1}{3!} \begin{vmatrix} s & 1 & 0 \\ p_2 - (1-s)^2 & s & 2 \\ p_3 - (1-s)^3 & p_2 - (1-s)^2 & s \end{vmatrix}. \quad (\text{C.7})$$

Based on the above observation, we obtain that

$$\begin{aligned} \Phi(x, y, z; s) &= (1-s)xyz = (1-s) \left( s^3 - 2s^2 + \frac{3-p_2}{2}s + \frac{p_3-1}{3} \right) \\ &= - \left( s^4 - 3s^3 + \frac{7-p_2}{2}s^2 + \frac{3p_2+2p_3-11}{6}s + \frac{1-p_3}{3} \right) \\ &\equiv \Phi(s|p_2, p_3). \end{aligned} \quad (\text{C.8})$$

Here, we use  $\Phi(s|p_2, p_3)$  to represent the second line of Eq. (C.8). For convenience, let  $P(s|p_2, p_3) = -\Phi(s|p_2, p_3)$ , and then the target problem is equivalently transformed to optimizing  $P(s|p_2, p_3)$  over the closed interval  $[s_{\min}, s_{\max}] (\subseteq [\frac{3}{4}, \frac{3}{2}])$  for any given pair  $(p_2, p_3) \in \mathcal{A}$ .

## D The optimization process of $P(s|p_2, p_3)$

We calculate the first and second derivatives of  $P(s|p_2, p_3)$  with respect to  $s$  as

$$\frac{d}{ds}P(s|p_2, p_3) = 4s^3 - 9s^2 + (7-p_2)s + \frac{3p_2+2p_3-11}{6}, \quad (\text{D.1})$$

$$\frac{d^2}{ds^2}P(s|p_2, p_3) = 12s^2 - 18s + (7-p_2). \quad (\text{D.2})$$

Consider the second derivative  $\frac{d^2}{ds^2}P(s|p_2, p_3)$  which is a quadratic function with respect to  $s$ . By calculation the discriminant of the quadratic equation  $\frac{d^2}{ds^2}P(s|p_2, p_3) = 0$  is  $48(p_2 - \frac{1}{4})$ . Since  $p_2 \in [\frac{1}{4}, 1]$ , the discriminant is always nonnegative. Thus, the two roots of the equation are

$$s_{\pm} = \frac{9 \pm \sqrt{3(4p_2-1)}}{12}. \quad (\text{D.3})$$

One can verify that  $s_- \in [\frac{1}{2}, \frac{3}{4}]$  and  $s_+ \in [\frac{3}{4}, 1]$  for  $p_2 \in [\frac{1}{4}, 1]$ . Due to  $s \in [s_{\min}, s_{\max}] \subseteq [\frac{3}{4}, \frac{3}{2}]$ , we conclude that  $\frac{d^2}{ds^2}P(s|p_2, p_3) \geq 0$  when  $s \in [s_+, 1]$ ; and  $\frac{d^2}{ds^2}P(s|p_2, p_3) \leq 0$  when  $s \in [\frac{3}{4}, s_+]$ . Next, we consider the distribution of all roots of the cubic equation  $\frac{1}{4}\frac{d}{ds}P(s|p_2, p_3) = 0$  with respect to  $s$ , namely

$$s^3 - \frac{9}{4}s^2 + \frac{7-p_2}{4}s + \frac{3p_2+2p_3-11}{24} = 0. \quad (\text{D.4})$$

Taking  $s = t + \frac{3}{4}$  in Eq. (D.4) we obtain that

$$t^3 + pt + q = 0, \quad (\text{D.5})$$



where

$$p = \frac{1-4p_2}{16}, \quad q = \frac{1-6p_2+8p_3}{96}. \quad (\text{D.6})$$

Its discriminant is given by  $D(p_2, p_3) = -108 \cdot \Delta(p_2, p_3)$ , where

$$\Delta(p_2, p_3) = \frac{q^2}{4} + \frac{p^3}{27} = \frac{1}{576} \left( p_3^2 + \frac{1-6p_2}{4} p_3 + \frac{1-12p_2+39p_2^2-16p_2^3}{48} \right) \quad (\text{D.7})$$

$$= \frac{1}{576} (p_3 - f^+(p_2)) (p_3 - f^-(p_2)), \quad (\text{D.8})$$

where  $f^\pm(p_2)$  are formulated in Eq. (2.3). It follows from Eq. (2.2) that  $p_3$  is bounded by  $f^\pm(p_2)$  for any two-qubit state. That is,  $f^-(p_2) \leq p_3 \leq f^+(p_2)$  for any fixed pair  $(p_2, p_3) \in \mathcal{A}$ . Hence, we conclude that  $\Delta(p_2, p_3) = 0$  if  $p_3 = f^+(p_2)$  or  $p_3 = f^-(p_2)$ , otherwise  $\Delta(p_2, p_3)$  is always negative. We also plot the surface graph in the  $(p_2, p_3, \Delta)$ -coordinate system, see Fig. 5, to perceive the sign of  $\Delta(p_2, p_3)$  more intuitively. Based on the sign of  $\Delta(p_2, p_3)$ , we shall investigate the distribution of all roots of the equation  $\frac{1}{4} \frac{d}{ds} P(s|p_2, p_3) = 0$  in two cases. The first case is when  $\Delta(p_2, p_3) = 0$ , and the second is when  $\Delta(p_2, p_3) < 0$ . Note that  $(p_2, p_3) \in \mathcal{A}$ , then  $p_2 = \frac{1}{4}$  implies that  $p_3 = \frac{1}{16}$ . Then it must be true that  $p = 0$  and  $q = 0$  at the same time. In a word, beyond the boundary of  $\mathcal{A}$ , we see that

$$p < 0 \quad \text{and} \quad \Delta < 0. \quad (\text{D.9})$$

In addition,  $q$  vanished only when the point  $(p_2, p_3)$  lies on the line  $p_3 = f(p_2) = \frac{6p_2-1}{8}$ .

(1) If  $\Delta(p_2, p_3) = 0$ , then  $p_3 = f^\pm(p_2)$  for  $p_2 \in [\frac{1}{4}, 1]$ . According to Appendix E, the three roots of the equation  $\frac{1}{4} \frac{d}{ds} P(s|p_2, p_3) = 0$  are all real. We further consider the following two subcases.

(1a) If  $p_3 = f^-(p_2)$ , then  $q < 0$  since  $f(p_2) > f^-(p_2)$ , the three roots of the equation  $\frac{1}{4} \frac{d}{ds} P(s|p_2, p_3) = 0$  comprise of one simple root and double root, respectively, which are given by the formulae:

$$\ell_+ := \frac{3}{4} + \frac{3q}{p} = \frac{9+2\sqrt{3(4p_2-1)}}{12} \quad \text{and} \quad \ell_- := \frac{3}{4} - \frac{3q}{2p} = \frac{9-\sqrt{3(4p_2-1)}}{12}. \quad (\text{D.10})$$

It implies that

$$\frac{1}{4} \frac{d}{ds} P(s|p_2, p_3) = (s - \ell_+) (s - \ell_-)^2, \quad (\text{D.11})$$

and all the three real roots are  $s_1 = \ell_+$  and  $s_2 = s_3 = \ell_-$ . One can verify only the root  $s_1 = \frac{9+2\sqrt{3(4p_2-1)}}{12} \in [\frac{3}{4}, \frac{3}{2}]$ . Hence, we only need to consider the stationary point with  $s = \ell_+$ . If  $\ell_+ \in [s_{\min}, s_{\max}]$ , then

$$\begin{aligned} \min_{s \in [s_{\min}, s_{\max}]} P(s|p_2, p_3) &= \min \{ P(\ell_+|p_2, f^-(p_2)), P(s_{\max}|p_2, f^-(p_2)), P(s_{\min}|p_2, f^-(p_2)) \}, \\ \max_{s \in [s_{\min}, s_{\max}]} P(s|p_2, p_3) &= \max \{ P(\ell_+|p_2, f^-(p_2)), P(s_{\max}|p_2, f^-(p_2)), P(s_{\min}|p_2, f^-(p_2)) \}. \end{aligned}$$

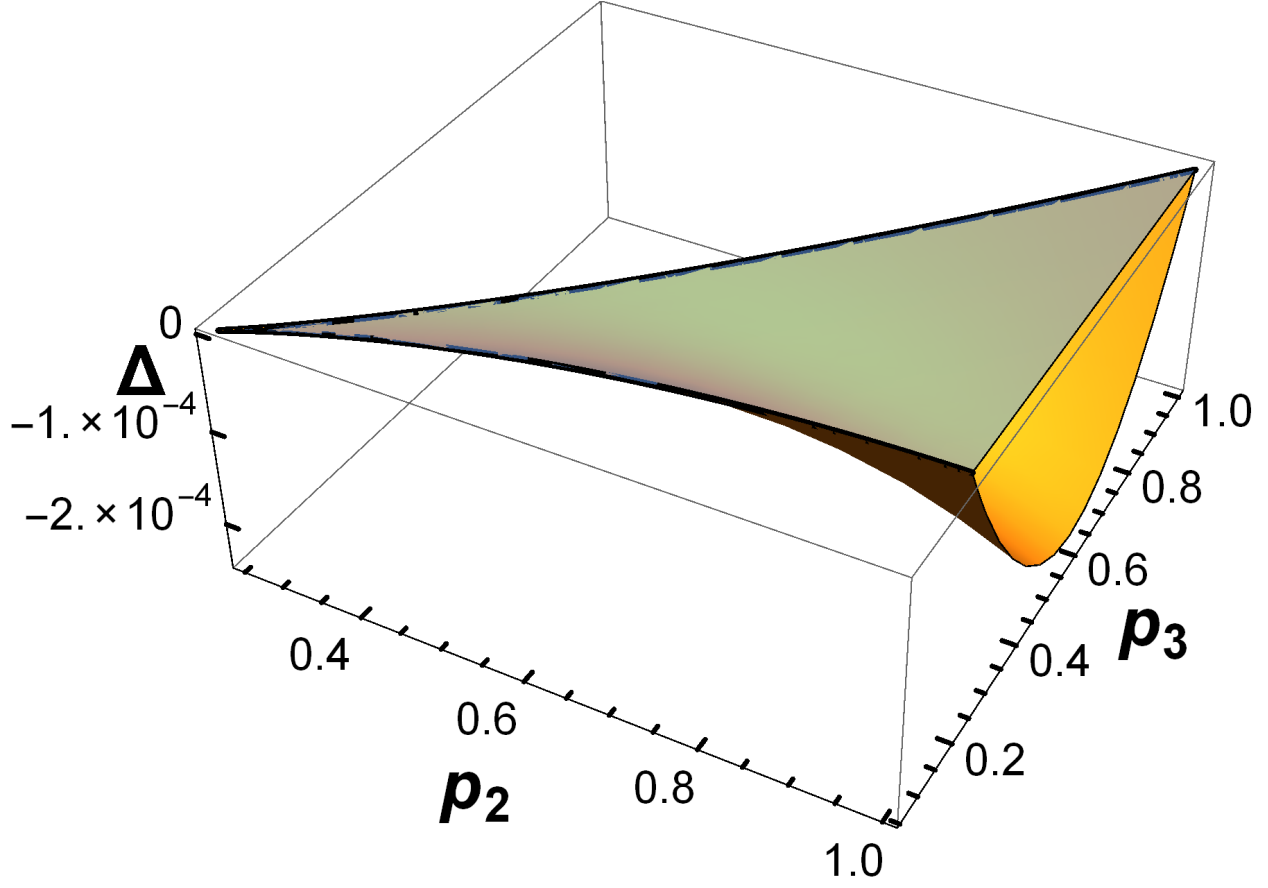


Figure 5: (Color Online) The surface corresponding to  $\Delta(p_2, p_3)$  supported on the 2D region  $\mathcal{A}$ . The surface below the plane of  $\Delta(p_2, p_3) = 0$  except the two boundary curves  $p_3 = f^\pm(p_2)$ . The two curves  $p_3 = f^\pm(p_2)$  both lie in the plane of  $\Delta(p_2, p_3) = 0$ .

Otherwise, if  $\ell_+ \notin [s_{\min}, s_{\max}]$ , then

$$\begin{aligned} \min_{s \in [s_{\min}, s_{\max}]} P(s|p_2, p_3) &= \min \{P(s_{\max}|p_2, f^-(p_2)), P(s_{\min}|p_2, f^-(p_2))\}, \\ \max_{s \in [s_{\min}, s_{\max}]} P(s|p_2, p_3) &= \max \{P(s_{\max}|p_2, f^-(p_2)), P(s_{\min}|p_2, f^-(p_2))\}. \end{aligned}$$

(1b) If  $p_3 = f^+(p_2)$ , then  $q > 0$  since  $f^+(p_2) > f(p_2)$ , the three roots of the equation  $\frac{1}{4} \frac{d}{ds} P(s|p_2, p_3) = 0$  comprise of one simple root and double root, respectively, which are given by the formulae:

$$L_- := \frac{3}{4} + \frac{3q}{p} = \frac{9 - 2\sqrt{3(4p_2 - 1)}}{12} \text{ and } L_+ := \frac{3}{4} - \frac{3q}{2p} = \frac{9 + \sqrt{3(4p_2 - 1)}}{12}. \quad (\text{D.12})$$

We see that

$$\frac{1}{4} \frac{d}{ds} P(s|p_2, p_3) = (s - L_-)(s - L_+)^2, \quad (\text{D.13})$$

are the three roots are  $s_1 = s_2 = L_+$  and  $s_3 = L_-$ . One can verify that only the double roots  $s_1 = s_2 = \frac{9+\sqrt{3(4p_2-1)}}{12} \in [\frac{3}{4}, 1]$ . Hence, we only need to consider the stationary point with  $s = L_+$ . If  $L_+ \in [s_{\min}, s_{\max}]$ , then

$$\begin{aligned} \min_{s \in [s_{\min}, s_{\max}]} P(s|p_2, p_3) &= \min \{P(L_+|p_2, f^+(p_2)), P(s_{\max}|p_2, f^+(p_2)), P(s_{\min}|p_2, f^+(p_2))\}, \\ \max_{s \in [s_{\min}, s_{\max}]} P(s|p_2, p_3) &= \max \{P(L_+|p_2, f^+(p_2)), P(s_{\max}|p_2, f^+(p_2)), P(s_{\min}|p_2, f^+(p_2))\}. \end{aligned}$$

If  $L_+ \notin [s_{\min}, s_{\max}]$ , then

$$\begin{aligned} \min_{s \in [s_{\min}, s_{\max}]} P(s|p_2, p_3) &= \min \{P(s_{\max}|p_2, f^+(p_2)), P(s_{\min}|p_2, f^+(p_2))\}, \\ \max_{s \in [s_{\min}, s_{\max}]} P(s|p_2, p_3) &= \max \{P(s_{\max}|p_2, f^+(p_2)), P(s_{\min}|p_2, f^+(p_2))\}. \end{aligned}$$

- (2) If  $\Delta(p_2, p_3) < 0$ , then  $f^-(p_2) < p_3 < f^+(p_2)$  for  $\frac{1}{4} < p_2 \leq 1$ . According to Appendix E, the cubic equation formulated in Eq. (D.5), with coefficients given by Eq. (D.6), has three real roots given by

$$\begin{cases} t_1 = \frac{\sqrt{3(4p_2-1)}}{6} \cos \theta \\ t_2 = \frac{\sqrt{3(4p_2-1)}}{6} \cos \left( \theta - \frac{2\pi}{3} \right) \\ t_3 = \frac{\sqrt{3(4p_2-1)}}{6} \cos \left( \theta + \frac{2\pi}{3} \right) \end{cases}, \quad (\text{D.14})$$

where

$$\theta \equiv \theta(p_2, p_3) = \frac{1}{3} \arccos \left( \frac{\sqrt{3}(6p_2 - 8p_3 - 1)}{(4p_2 - 1)^{\frac{3}{2}}} \right). \quad (\text{D.15})$$

Recall that  $\frac{1}{4} \frac{d}{ds} P(s|p_2, p_3) = 0$  can be transformed to Eq. (D.5) by taking  $s = t + \frac{3}{4}$ . It follows that  $\frac{1}{4} \frac{d}{ds} P(s|p_2, p_3) = 0$  has three real roots given by

$$\begin{cases} s_1 = r_1(p_2, p_3) := \frac{3}{4} + \frac{\sqrt{3(4p_2-1)}}{6} \cos \theta \\ s_2 = r_2(p_2, p_3) := \frac{3}{4} + \frac{\sqrt{3(4p_2-1)}}{6} \cos \left( \theta - \frac{2\pi}{3} \right) \\ s_3 = r_3(p_2, p_3) := \frac{3}{4} + \frac{\sqrt{3(4p_2-1)}}{6} \cos \left( \theta + \frac{2\pi}{3} \right) \end{cases}. \quad (\text{D.16})$$

The local extreme values can be attained only at the stationary points and boundary points. In order to roughly determine the values of these roots for a fixed pair  $(p_2, p_3) \in \mathcal{A}$ , we plot the 3D surfaces of the above three roots  $s_i = r_i(p_2, p_3)$ , where  $i = 1, 2, 3$ , in terms of  $p_2$  and  $p_3$ , see Fig. 6.

Combining the two cases investigated above, we find that for any pair  $(p_2, p_3) \in \mathcal{A}$ , the three roots of  $\frac{1}{4} \frac{d}{ds} P(s|p_2, p_3) = 0$  in the descending order, i.e.  $r_1 \geq r_2 \geq r_3$ , satisfy that

$$\frac{1}{4} \leq r_3 \leq \frac{3}{4} \leq r_1 \leq \frac{5}{4} \quad \text{and} \quad \frac{1}{2} \leq r_2 \leq 1. \quad (\text{D.17})$$

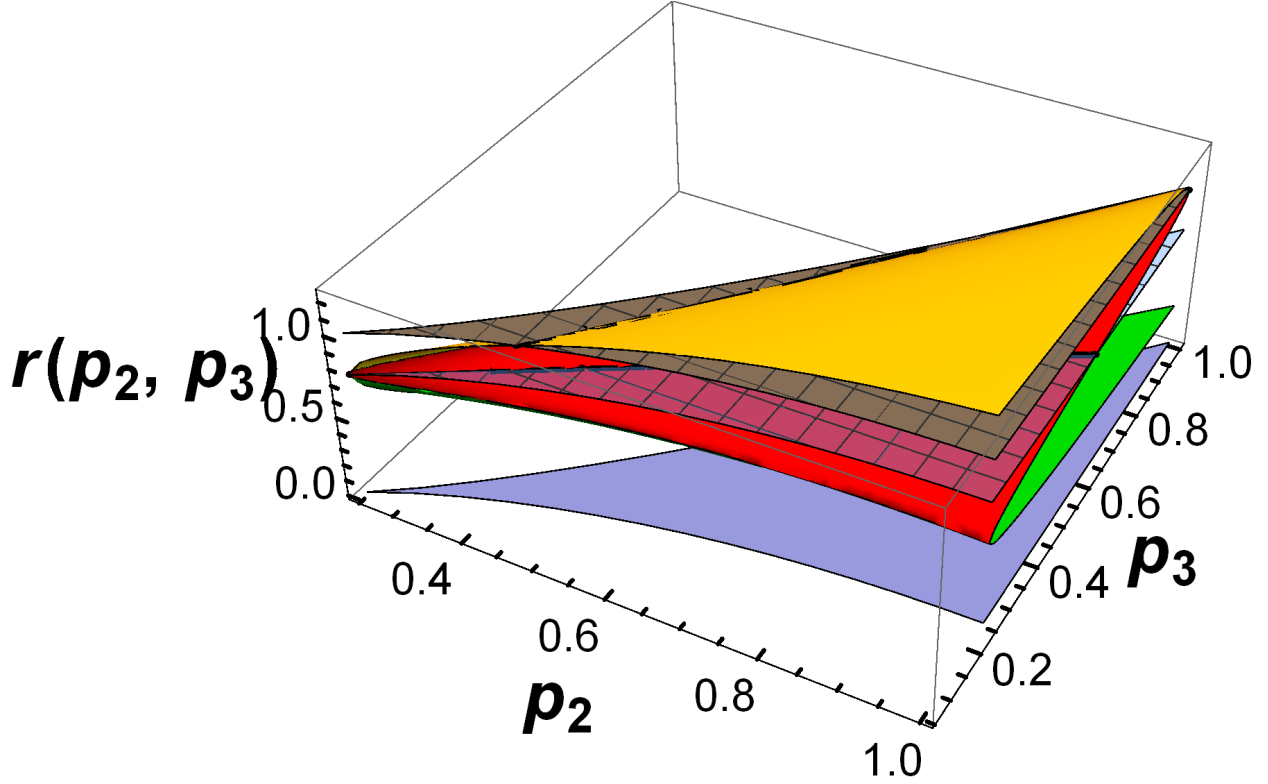


Figure 6: (Color Online) The three distinct real roots  $r(p_2, p_3)$  of the cubic equation  $\frac{1}{4} \frac{d}{ds} P(s|p_2, p_3) = 0$  for any pair  $(p_2, p_3) \in \mathcal{A}$ . The root  $r(p_2, p_3) = 1$  stands for the line  $p_3 = \frac{3p_2-1}{2}$  with  $p_2 \in [\frac{7}{16}, 1]$ , and the root  $r(p_2, p_3) = \frac{3}{4}$  stands for the line  $p_3 = \frac{6p_2-1}{8}$  with  $p_2 \in [\frac{1}{4}, 1]$ .

In particular, according to the first case when  $p_3 = f^\pm(p_2)$ , we determine that  $r_1 = r_2 \in [\frac{3}{4}, 1]$  on the upper boundary curve of  $\mathcal{A}$ , i.e.  $p_3 = f^+(p_2)$ , and  $r_2 = r_3 \in [\frac{1}{2}, \frac{3}{4}]$  on the lower boundary curve of  $\mathcal{A}$ , i.e.  $p_3 = f^-(p_2)$ . In addition, we find that  $r_1(p_2, p_3) = 1$  determines a curve  $p_3 = \frac{3p_2-1}{2}$  in the 2D region of  $\mathcal{A}$ , where  $p_2 \in [\frac{7}{16}, 1]$ , and  $r_2(p_2, p_3) = \frac{3}{4}$  determines a curve  $p_3 = \frac{6p_2-1}{8}$ , where  $p_2 \in [\frac{1}{4}, 1]$ .

## E Cardano formula

The Cardano formula is named after G. Cardano, who was the first to publish it in 1545. This formula is one for finding the roots of the general cubic equation over  $\mathbb{C}$ . In our paper, we are interested in those cubic equations whose all roots are real. For such class of cubic equations to be used in optimization, Bauschke, Lal, and Wang give a thorough consideration in their recent paper [21]:

**Theorem E.1.** *Let  $f(x) := x^3 + px + q$ , where both  $p$  and  $q$  are in  $\mathbb{R}$ . Then 0 is the only inflection point*

of  $f$ :  $f$  is strictly concave on  $(-\infty, 0)$  and  $f$  is strictly convex on  $(0, +\infty)$ . Moreover, exactly one of the following occurs:

(i)  $p < 0$ : Set  $x_{\pm} := \sqrt{-\frac{p}{3}}$ . Then  $x_- < x_+$ , where  $x_{\pm}$  are two distinct simple roots of the equation  $f'(x) = 0$ ,

- $f$  is strictly increasing on  $(-\infty, x_-]$ ;
- $f$  is strictly decreasing on  $[x_-, x_+]$ ;
- $f$  is strictly increasing on  $[x_+, +\infty)$ .

Moreover,

$$f(x_+)f(x_-) = 4\Delta, \quad \Delta := \left(\frac{p}{3}\right)^3 + \left(\frac{q}{2}\right)^2, \quad (\text{E.1})$$

and this case trifurcates further as follows:

(a)  $\Delta > 0$ : Then the equation  $f(x) = 0$  has **exactly one real root**  $r$ . It is simple and given by

$$r := u_- + u_+, \quad u_{\pm} := \left(-\frac{q}{2} \pm \sqrt{\Delta}\right)^{\frac{1}{3}}. \quad (\text{E.2})$$

The remaining **two simple nonreal roots** are given by

$$\frac{-(u_- + u_+) \pm \sqrt{-3}(u_- - u_+)}{2}. \quad (\text{E.3})$$

(b)  $\Delta = 0$ : If  $q > 0$  ( $q < 0$ ), then  $2x_-$  ( $2x_+$ ) is a **simple real root** while  $x_+$  ( $x_-$ ) is a **double real root**. Moreover, these cases can be combined into

- $3\frac{q}{p} = 2\left(-\frac{q}{2}\right)^{\frac{1}{3}}$  is a **simple root** of the equation  $f(x) = 0$ , and
- $-\frac{3q}{2p} = -\left(-\frac{q}{2}\right)^{\frac{1}{3}}$  is a **double root** of the equation  $f(x) = 0$ .

(c)  $\Delta < 0$ : Then the equation  $f(x) = 0$  has **three simple real roots**:  $r_-, r_0, r_+$ , where  $r_- < z_- < r_0 < z_+ < r_+$ . Indeed, set

$$\theta := \arccos \left[ \left(-\frac{q}{2}\right) \left(-\frac{p}{3}\right)^{-\frac{3}{2}} \right], \quad (\text{E.4})$$

which lies in  $(0, \pi)$ , and then define  $x_k$  ( $k = 0, 1, 2$ ) by

$$x_k := 2\sqrt{-\frac{p}{3}} \cos \left( \frac{\theta + 2k\pi}{3} \right). \quad (\text{E.5})$$

Then  $r_- = x_1, r_0 = x_2$ , and  $r_+ = x_0$ .

(ii)  $p = 0$ : Then the equation  $f'(x) = 0$  has a **double root** at 0, and  $f$  is strictly increasing on  $\mathbb{R}$ . The only real root is given by

$$r := \sqrt[3]{-q}. \quad (\text{E.6})$$

If  $q = 0$ , then  $r$  is a triple root. If  $q \neq 0$ , then  $r$  is a simple root and the remaining nonreal simple roots are given by  $\frac{-1 \pm \sqrt{-3}}{2}r$ .

(iii)  $p > 0$ : Then the equation  $f'(x) = 0$  has no real root,  $f$  is strictly increasing on  $\mathbb{R}$ , and  $f$  has **exactly one real root**  $r$ . It is simple and given by

$$r := u_- + u_+ \quad (\text{E.7})$$

where  $u_{\pm} := \left(-\frac{q}{2} \pm \sqrt{\Delta}\right)^{\frac{1}{3}}$  and  $\Delta := \left(\frac{p}{3}\right)^3 + \left(\frac{q}{2}\right)^2$ .

Once again, the remaining **two simple nonreal roots** are

$$r := u_- + u_+, \quad u_{\pm} := \left(-\frac{q}{2} \pm \sqrt{\Delta}\right)^{\frac{1}{3}}. \quad (\text{E.8})$$

**Proposition E.2.** Given a cubic equation with real coefficients:

$$x^3 + a_2x^2 + a_1x + a_0 = 0 \quad (a_0 \neq 0), \quad (\text{E.9})$$

it follows that Eq. (E.9) must have at least one real root. In particular,

(i) Let  $\gamma$  is a real root of Eq. (E.9). Then we have

$$\frac{x^3 + a_2x^2 + a_1x + a_0}{x - \gamma} = x^2 + (a_2 + \gamma)x - \frac{a_0}{\gamma}. \quad (\text{E.10})$$

Thus the last two roots are given by

$$\frac{-(a_2 + \gamma)\gamma \pm \sqrt{(a_2\gamma + \gamma^2)^2 + 4a_0\gamma}}{2\gamma}. \quad (\text{E.11})$$

(ii) Let  $\alpha, \beta$  be two real roots of Eq. (E.9). Then all roots of Eq. (E.9) must be real, and we have

$$\frac{x^3 + a_2x^2 + a_1x + a_0}{(x - \alpha)(x - \beta)} = x + a_2 + \alpha + \beta. \quad (\text{E.12})$$

Thus the last real root must be  $-(a_2 + \alpha + \beta)$ .

*Proof.* (i) Note that

$$\begin{aligned} \frac{x^3 + a_2x^2 + a_1x + a_0}{x - \gamma} &= x^2 + (a_2 + \gamma)x + (\gamma^2 + a_2\gamma + a_1) + \frac{\gamma^3 + a_2\gamma^2 + a_1\gamma + a_0}{x - \gamma} \\ &= x^2 + (a_2 + \gamma)x + (\gamma^2 + a_2\gamma + a_1), \end{aligned}$$

where we used the fact that  $\gamma$  is the real root of Eq. E.9, i.e.,  $\gamma^3 + a_2\gamma^2 + a_1\gamma + a_0 = 0$ . Then  $\gamma^2 + a_2\gamma + a_1 = -\frac{a_0}{\gamma}$  follows from the fact that  $\gamma \neq 0$  due to  $a_0 \neq 0$ . Therefore, we get that

$$\frac{x^3 + a_2x^2 + a_1x + a_0}{x - \gamma} = x^2 + (a_2 + \gamma)x - \frac{a_0}{\gamma}.$$

(ii) The proof goes similarly as to (i). Indeed,

$$\begin{aligned} \frac{x^3 + a_2x^2 + a_1x + a_0}{(x - \alpha)(x - \beta)} &= (x + a_2 + \alpha + \beta) + \frac{\alpha^3 + a_2\alpha^2 + a_1\alpha + a_0}{(\alpha - \beta)(x - \alpha)} + \frac{\beta^3 + a_2\beta^2 + a_1\beta + a_0}{(\beta - \alpha)(x - \beta)} \\ &= x + a_2 + \alpha + \beta, \end{aligned}$$

which finishes the proof. □